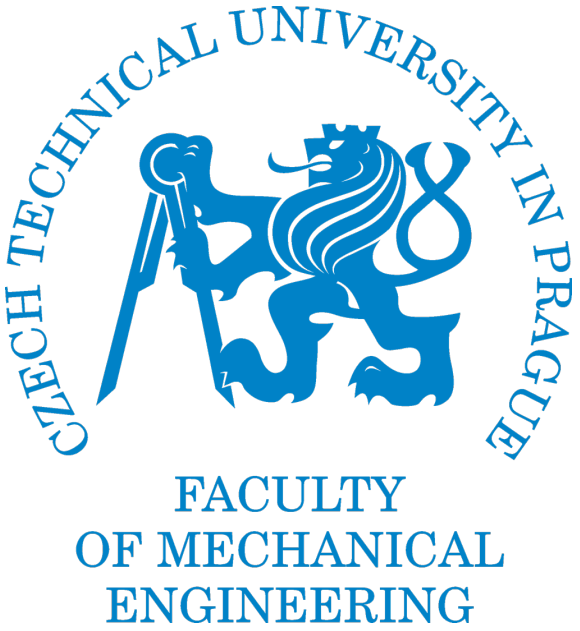

Aerodynamics of Bodies at Very High Mach Numbers

Bachelor of Science Thesis

For obtaining the degree of Bachelor of Science in Mechanical Engineering
at Czech Technical University in Prague

Hyoungju Lee

July 9, 2023

Faculty of Mechanical Engineering · Czech Technical University in Prague

BACHELOR'S THESIS ASSIGNMENT

I. Personal and study details

Student's name: **Lee HyoungJu** Personal ID number: **456089**

Faculty / Institute: **Faculty of Mechanical Engineering**

Department / Institute: **Department of Fluid Dynamics and Thermodynamics**

Study program: **Theoretical Fundamentals of Mechanical Engineering**

II. Bachelor's thesis details

Bachelor's thesis title in English:

Aerodynamics of Bodies at Very High Mach Numbers

Bachelor's thesis title in Czech:

Aerodynamika těles při velmi vysokých hodnotách Machova čísla

Guidelines:

1) Perform theoretical analysis in the field of super/hypersonic aerodynamics (basic equations, basic principles, the difference between super/hyper sonic flow, etc.).
2) Describe CFD methods and conditions for use in hypersonic flow.
3) Design a simple aerodynamic body for hypersonic velocity.
4) Perform CFD analysis on the designed body with the evaluation of its lift and drag forces as well as velocity field and temperature field.
5) Compare the results of your calculations (simulations) with the data in scientific literature.

Bibliography / sources:

- SHAPIRO, A.H. 1953. The dynamics and thermodynamics of compressible fluid flow. New York: The Ronald Press Company.
- ANDERSON, J.D. 1990. Modern compressible flow - With historical perspective. McGraw-Hill. ISBN: 0-07-001673-9.
- NASA Technical Reports

Name and workplace of bachelor's thesis supervisor:

Ing. Michal Schmirler, Ph.D. Department of Fluid Dynamics and Thermodynamics FME

Name and workplace of second bachelor's thesis supervisor or consultant:

Date of bachelor's thesis assignment: **25.04.2023** Deadline for bachelor thesis submission: **28.07.2023**

Assignment valid until: _____

Ing. Michal Schmirler, Ph.D. Supervisor's signature	Ing. Michal Schmirler, Ph.D. Head of department's signature	doc. Ing. Miroslav Španiel, CSc. Dean's signature

III. Assignment receipt

The student acknowledges that the bachelor's thesis is an individual work. The student must produce his thesis without the assistance of others, with the exception of provided consultations. Within the bachelor's thesis, the author must state the names of consultants and include a list of references.

Date of assignment receipt	Student's signature

Declaration

I declare that presented thesis called “Aerodynamics of Bodies at Very High Mach Numbers” made under supervision of Ing. Michal Schmirler, Ph.D., was written by me using literatures listed in the chapter “Bibliography”.

Thesis Title:	Aerodynamics of Bodies at Very High Mach Numbers	
Author:	Hyoungju Lee	
Year:	2023	
Study Program:	Theoretical Fundamentals of Mechanical Engineering	
Type of the Thesis:	Bachelor's	
Name of supervisor:	Michal Schmirler	
Name of the second supervisor:	Jiri Teichman	
Bibliographic data:	Number of pages	49
	Number of figures	40
	Number of tables	8
	Number of attachments	
Keywords	Hypersonic, Mach number, Boundary layers	

Abstract:

This thesis work attempts to reproduce the NASA experiment regarding the aerodynamics of bodies at high Mach numbers 11.5, 19.5, and 34, using CFD simulation on Ansys Fluent software and compare the results to evaluate the accuracy of the simulation. Theoretical frameworks of hypersonic flow regime are presented with basic equations and principles, as well as appropriate CFD methods and conditions are going to be selected according to the body that was used in NASA experiment.

Acknowledgement

I would like to thank my supervisors, Michal Schmirler and Jiri Teichman, for sharing their knowledge and guiding me through a complete the bachelor thesis project. Being able to have the access to the powerful computing device from Department of Fluid Dynamics and Thermodynamics and the necessary guidance under Prof. Schmirler is one of the privileges that I could experience. Furthermore, I express my gratitude towards Jiri Teichman for his help with Ansys Fluent with his advanced knowledge. Lastly, I would like to thank my family and partner, for giving me love and support for whole 3 years of bachelor's degree, and beyond.

Prague,
July 17, 2023

Hyoungju Lee

Symbols

Latin Symbols

c_p	Specific heat at constant pressure	[J·kg^{-1}·K^{-1}]
c_v	Specific heat at constant volume	[J·kg^{-1}·K^{-1}]
C_D	Drag coefficient	[1]
C_L	Lift coefficient	[1]
C_m	Moment coefficient	[1]
d	Reference diameter, model base	[m]
R	Gas constant	[J·K^{-1}·mol^{-1}]
M	Mach number	[1]
M_∞	Free-stream Mach number	[1]
p	Pressure	[N/m^2]
p_c	Inviscid surface pressure	[N/m^2]
q	Heat flux	[W/m^2]
q_∞	Radiative heat flux	[W/m^2]
Re_x	Local Reynolds number	[1]
T	Temperature	[K]

Greek Symbols

δ	Boundary layer thickness	[m]
γ	Specific heat ratio	[1]
θ	Surface inclination angle	[rad]
λ	Mean free path	[m]
μ	Dynamics viscosity	[kg·m^{-1}·s^{-1}]
ρ	Density	[kg/m^3]

Abbreviations

AoA	Angle of Attack
CFD	Computational Fluid Dynamics
CAD	Computer-Aided Design
DLR	Deutsches Zentrum für Luft-und Raumfahrt
DNS	Direct Numerical Simulation
DO	Discrete ordinates
ESA	European Space Agency
NASA	National Aeronautics and Space Administration
RANS	Reynold-Averaged Navier-Stokes equation
RTE	Radiative Transfer Equation
SST	Shear Stress Transport
TN	Technical Note

Table of Contents

Section 1

Introduction

"The best thing that any businessman can do with his few hours saved by flying supersonically is to have a few more Martinis". This is what 'New Scientist', a science magazine, criticized the first supersonic commercial airplane Concorde in 1971 for its absurdness. Since then, a seed of high-speed flying vehicle had been planted in people's mind. [1]

And about 10 years later, a new future had been presented to the world by Ronald Reagan during his State of the Union Address in 1986. He envisioned that a new Orient Express takes off from Dulles Airport, accelerates up to at least 25 times the speed of sound, and lands in Tokyo two hours later, making the world reachable within few hours distance. This is what Ronald Reagan imagined by the end of the 90s when he held the State of the Union in his hand. The reality is, however, this vision has not arrived yet. [2]

At the time of writing, hypersonic flight, both manned and unmanned, has been successfully achieved. However, practical hypersonic flight is not a commonplace yet, especially, the era of hypersonic vehicle is still ahead of us. Thus, there has to be more studies should be carried out about the topic of hypersonic flow related to stability of its vehicle, and more evaluations need to be done in order to verify them.

1.1 Previous work

The studies related to stability of hypersonic object have been carried out by different research institutions including DLR (German space agency), ESA (European Space Agency), and NASA (National Aeronautics and Space Administration).

According to NASA TN Number D-3193, research regarding to stability and drag of bodies at different Mach numbers was conducted in 1966. The geometries used in this

experiment were a pointed and a blunted half-angle cone with aluminum and Telfon as materials.
The drag characteristics, static-stability characteristics, and dynamic-stability characteristics were evaluated using the experimental values. [3]

1.2 Thesis goal

As it was presented in the previous section, the experiment should be verified. Thus, this thesis will focus on using CFD simulation software to regenerate and realize the results of stability which has been studied during the experiment in NASA TN. The results from the simulation can then be compared to NASA paper to evaluate the accuracy of the simulation. The goal of the thesis is defined as follows:

Reproduce the NASA experiment using CFD simulation.

The subgoals to achieve this main goal are as follows:

1. Definition of hypersonic flow,
2. select and validate suitable boundary conditions and settings for hypersonic flow simulations,
3. perform hypersonic flow simulation at different angles of attack and Mach numbers,
4. compare the simulation results.

Then, the main thesis question is defined as follows:

Compared to the data between NASA technical note, how accurate the CFD simulation is?

To answer this main thesis question, different subquestions are formulated. These subquestions will give a better understanding of the problem, therefore contributing to answer the main question.

1. How similar the shockwaves from both NASA TN and simulation?
2. How accurate the drag coefficients are compared to that of NASA TN?
3. How accurate the pith-moment coefficients are compared to that of NASA TN?

1.3 Report structure

This section is an introductory section the previous work from NASA and thesis goal were presented. In section 2, the background descriptions regarding hypersonic flow that are considered to be necessary in this thesis to provide better understanding.

Since the good understanding of the CFD software is crucial in this thesis work, chapter 3 is focused on validation of boundary conditions, settings, and solver methods based on Ansys Fluent user guide. Section 3.1 defines the geometry that is evaluated in the simulation and boundary conditions to validate the hypersonic flow regime. Section 3.2 provides the general frameworks regarding the selected settings and their suitability in terms of hypersonic calculations.

With the use of NASA TN Number D-3193 (1966), results regarding hypersonic flow at different Mach numbers and AoAs have been obtained. Section 4 presents the results and compares them with the NASA TN.

With all the information from section 2 to 4, the thesis goal and question will be answered. Section 5 concludes the answers to all the subquestions.

Finally, the discussion for future research will be given in Section 6.

Section 2

Theoretical Analysis in the Hypersonic Flow

This section is dedicated to explaining general hypersonic aerodynamics. Generally speaking, hypersonic aerodynamics are defined as those flows where the Mach number M is greater than 5. However, Mach number is not the only parameter that has to be considered to distinguish hypersonic aerodynamics from conventional supersonic aerodynamics. For instance, when Mach number increased from $M = 4.99$ to $M = 5.01$, there are no such dramatic changes. Yet, it is more important to pay attention to certain physical phenomena rather than Mach number itself. Therefore, hypersonic flow is best defined as "that regime where certain physical flow phenomena become progressively more important as the Mach number is increased to higher values". [4]

2.1 Thin shock layers

Not only the Mach number M itself is the measure of distinguishing the flow regime, but also there are few other factors that need to be considered. First of all, compared to any other than other flow regime, there are a quite thin shock layers created when object is going through the hypersonic flow regime. From the oblique shock theory which explains the phenomena about the shock wave created when a body encounters a flow at some angle, at some deflection angle the density increase across the shock wave becomes larger as the Mach number increases. And at higher density, the mass flow behind the shock can be fitted smaller area. This means that for a hypersonic flow body the distance between the body and the shock wave can be small. The gap between the body and the shock wave is called the *shock layer*, and for hypersonic speeds this shock layer can be quite thin due to higher density.

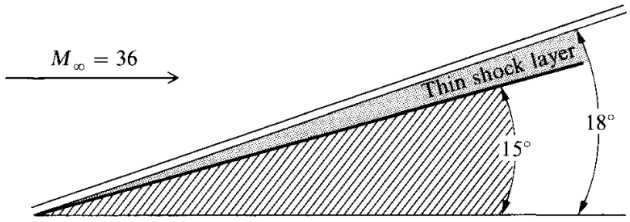

Figure 1. Thin Hypersonic Shock Layer *[4]*

Figure 1 illustrates the situation where the Mach 36 flow of a perfect gas over a 15-deg half angled wedge. As it was mentioned earlier, the shock wave angle will be only 18 degrees due to its higher density in this flow field.

2.2 Entropy layer

Secondly, the entropy layer along the body differentiates the hypersonic flow from the others. In case of a blunted cone as in the Fig 2, at hypersonic Mach number, the shock wave on the blunt nose is very thin, with a shock-detachment distance *d*. And in this nose region, the curvature of the shock wave is high. The entropy of the flow is known to be increased throughout a shock wave, so that as the shock wave gets stronger, the entropy increase gets also larger.

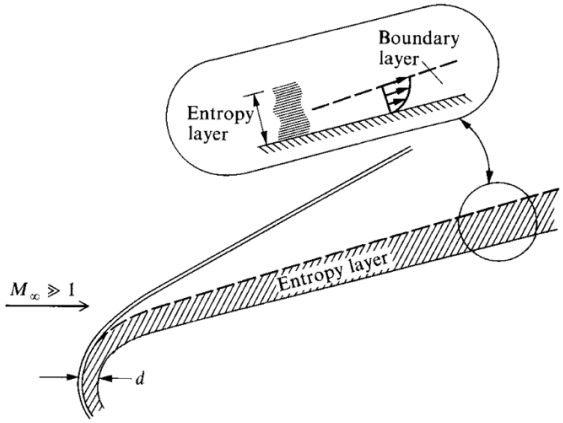

Figure 2. Entropy layer *[4]*

When a streamline passes through the strong, nearly normal portion of the curved shock wave near its centerline of the flow experiences a large entropy increase. This increase is much stronger than the one of a neighboring streamline passing through further away from the centerline of the flow. Thus, in the area of nose, there will be strong entropy gradients which will create and affect the entropy layer along the surface of the body for large distances from the nose as can be seen in Figure 2. In addition, the boundary layer along the surface grows within this entropy layer and is affected by it as well. [4]

2.3 Viscous interaction

Thirdly, viscous interaction within the boundary layer also differentiates the hypersonic regime from conventional flow regime.

Consider the hypersonic flow along a flat plate as it is described in Fig 3. A hypersonic flow, at a high velocity, the amount of kinetic energy contains a large amount of kinetic energy. And this large amount of kinetic energy is transformed into an internal energy of the gas due to viscous effects within the boundary layer which slows the hypersonic flow. As a result, the temperature within the boundary layer increases as in Figure 3 which shows a typical temperature profile in the boundary layer.

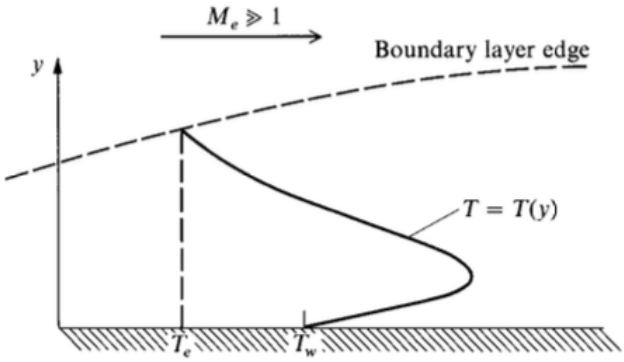

Figure 3. Temperature profile in a hypersonic boundary layer *[4]*

Such temperature increase dominates the characteristics of hypersonic boundary layers. For example, as the temperature increases the viscosity coefficient also increases which makes the boundary layer thicker. In addition, according to the equation of state $\rho = p/RT$, because the pressure p is constant in the normal direction of in the boundary layer, when the temperature T increases the density ρ decreases. As a result, to reach a certain amount of mass flow at reduced density, the thickness of the boundary layer should be larger.

Both decrease in the viscous coefficient and increase in the boundary-layer thickness make hypersonic boundary layers grow even faster than at slower speeds. This phenomenon can also be proved by following equation as

$$\delta \propto \frac{{M_\infty}^2}{\sqrt{Re_x}}$$

where δ is flat-plate compressible laminar boundary-layer thickness, M_∞ is the freestream Mach number and Re_x is the local Reynolds number. Since the thickness δ depends on the square of M_∞, it becomes extraordinarily large at hypersonic speeds. [4] This thick boundary layer in hypersonic flow can cause a major displacement effect on the inviscid flow outside the boundary layer and a body can appear much bigger than its actual size. Because the outer inviscid flow is influenced by the extreme thickness of the boundary layer flow, the changes in inviscid flow also can affect the growth of boundary layer. This interchangeable interaction between the boundary layer and the inviscid flow is called 'viscous interaction'. This interaction can influence on the surface-pressure distribution, in other words, lift, drag, and stability on hypersonic vehicles. Furthermore, due to viscous interaction, skin friction and heat transfer are also increased.

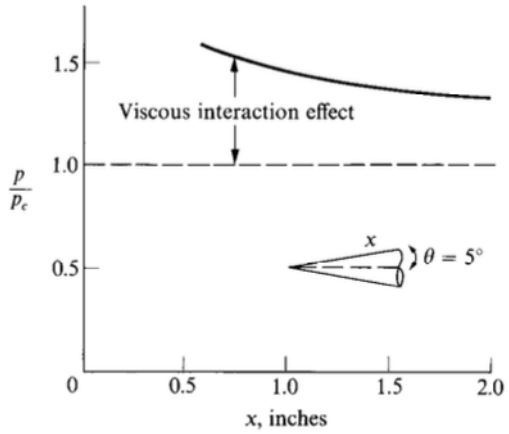

Figure 4. Viscous interaction effect. M_∞ = 11 / Re = 57302.4 per m *[4]*

Figure 4 shows the viscous interaction on a sharp cone with an angle of attack at zero degree. In Figure 4, the pressure distribution on the cone surface p is expressed as a function of distance from the tip. The inviscid surface pressure would be constant at p_c which is illustrated as the dashed line) if there is no viscous interaction between the boundary layer and inviscid flow. However, due to the viscous interaction, the pressure closer to the nose is relatively greater than the one along the cone surface which are further from the nose which approaches the inviscid value.

To be exact, when the boundary layer on a hypersonic vehicle becomes considerably thick so that it merges with the shock wave, a merged shock layer, the shock layer must be treated as fully viscous, and this is when the conventional boundary layer analysis should be neglected. [4]

2.4 High-temperature flow

Fourthly, hypersonic flow is also characterized as high-temperature flow. As it was discussed earlier, due to the friction within a boundary layer, the kinetic energy is dissipated within the boundary layer as well. And this viscous dissipation occurring within hypersonic boundary layers generates high temperature which is enough to cause the chemical change in gas. This high temperature excites the internal vibrational energy between the molecules of the gas which causes dissociation and even ionization. In addition, since general hypersonic vehicles are protected by an ablative heat shield, the ablation process also causes complex hydrocarbon chemical reactions. Due to these two reasons, there exists so called a *chemically reacting boundary layer* on the surface of a hypersonic vehicle.

However, the boundary layer is not the only region where the temperature reaches to the high manner around the hypersonic body. In the nose region of a blunt body, as illustrated in Figure 5, the bow shock wave is normal to the nose, and the temperature of the gas behind the shock wave can be extremely high at hypersonic speeds.

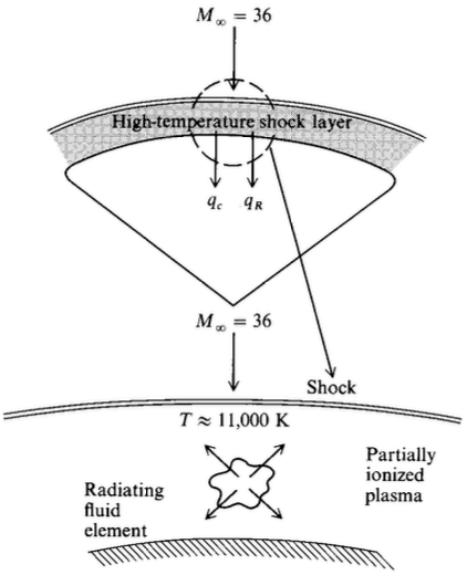

Figure 5. High-temperature shock layer *[4]*

This high-temperature situation behind the normal shock wave is well described in Figure 6.

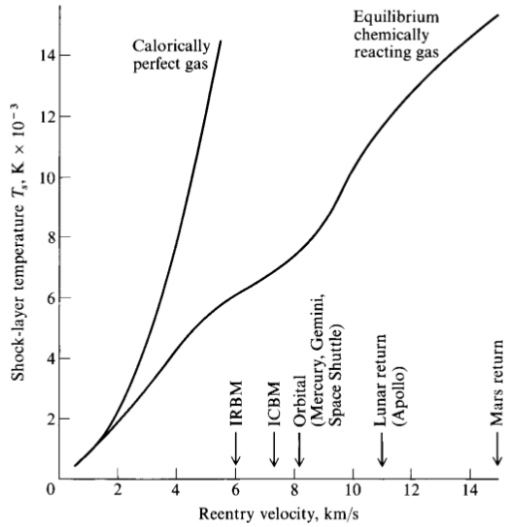

Figure 6. Temperature behind a normal shock wave at altitude of 52 km *[4]*

The upper curve shows an unrealistically high temperature value with a calorically perfect nonreacting gas and the specific heat constant at $\gamma = 1.4$. And the lower curve shows the situation which is closer to the actual situation by assuming an equilibrium chemically reacting gas. And from these two different situations following important points can be addressed:

- In any situation, the temperature in the nose region of a hypersonic body can be extremely high.
- The proper evaluation of effects of chemical reaction within the shock wave is crucial to identify an accurate shock-layer temperature. In other words, assumption of γ at 1.4 is no longer valid.

Thus, for a hypersonic flow, not only the boundary layer will be chemically reacting, but also the entire shock wave will be dominated by *chemically reacting flow*.

In a compressible flow which the specific heat constant of the gas is assumed to be constant, so that the ratio $\gamma = c_p/c_v$ is also constant. However, when the temperature of the gas increases to high values, the properties of the gas changes and it behaves in a nonideal manner. To be specific, the vibrational energy of the gas molecules becomes excited due to the temperature, as a result specific heats c_p and c_v become a function of temperature. Since specific heats influenced by the temperature the ratio γ also becomes a function of temperature.

As was mentioned above, the vibrational energy of the molecules becomes excited and causes chemical reaction to occur. And for general air, these chemical reactions are occurring above 800 K. Air is consisted of oxygen (O_2) and nitrogen (N_2), and as gas temperature in further increased above 800 K, the specific heats c_p and c_v become function of both temperature and pressure. At 2000 K, O_2 dissociation (O_2 -> 2O) begins which breaks the molecule apart into two atoms (2 O) and fully dissociated at 4000 K. In

case of Nitrogen (N_2), at 4000 K dissociation begins (N_2 -> 2N) and totally dissociated at 9000 K. Also, the air is completely dissociated and starts to ionize at 9000 K which allows electrons (e^-) moves freely so that makes both nitrogen and oxygen ions become positively charged (N^+ and O^+). As a result, ions are formed ($N \rightarrow N^+ + e^-$, and $O \rightarrow O^+ + e^-$) having enough energy to react with the surface of the vehicle.

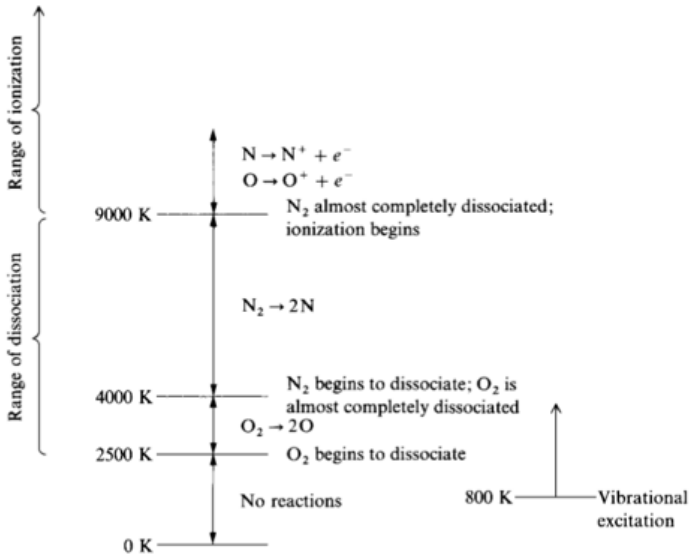

Figure 7. Range of vibrational excitation, dissociation, and ionization for air at 1 atm pressure *[4]*

All these physical and chemical phenomena are called high-temperature effects. Thus, in can be said, high-temperature effects can dominate one of the aspects of hypersonic aerodynamics. [4]

2.5 Low-density flow

Lastly, hypersonic flow can be characterized as a low-density flow. Individual molecules of the air collide over some period time and there will be some *average* distance the molecules move in order to be collided to successive ones. This average distance is denoted by λ, and it's defined as the *mean free path*. At standard sea-level, this mean free path $\lambda = 6.632448 \times 10^{-8}$m which is very small distance. However, at altitude about 98755.2 m, for example, where the density of the air is much lower, the average distance between the air molecules is significantly larger than that of at standard sea-level. The mean free path at altitude of 98755.2 m is $\lambda = 0.3048$ m.

At the altitude at sea-level, since the density of air molecules is high, the distance between the molecules is very small and it almost feels like a continuous medium. And this medium can be described as *continuum*. However, at high altitude, for example at 324,000 ft, the

molecules of the air are separated with larger distance, and the medium is no longer continuum. Under these conditions, the assumptions of a continuum begin to break down including concepts of the aerodynamics and equations. In this situation, the analysis of aerodynamics should be conducted from a different point of view using kinetic theory. This high altitude with non-continuum regime of aerodynamics where concept of kinetic theory starts to play a role is called *low-density flow*.
Due to low-density characteristic of hypersonic flow becomes more significant as the altitude increases, there are few assumptions of a continuum flow become tenuous. No-slip condition in the conventional viscous flow, the speed of the flow with the contact with the boundary is identical to the velocity of the boundary, begins to fail at certain high altitude. Instead, due to the low-density flow characteristic, the flow velocity at the boundary starts to have a finite value. This condition is called *velocity-slip condition*. In addition to this, the temperature of the gas at the boundary which normally taken as equal to that of the surface has different value. This is called *temperature-slip condition*. However, as the altitude continuously increases, it reaches to the point where the continuum-flow equations are no longer valid. And the air density will decrease even further down, so that there will be only a few molecules impact the surface per unit time. Thus, the mean free path between the molecules becomes even larger, and they do not collide/interact with other molecules. This flow regime is called *free molecule flow*.

Therefore, hypersonic flow can be visualized a body moving from a rarified atmosphere to a denser one, and that will shift the body from the *free molecule flow regime* where the importance of an individual molecular impact is crucial, to the *transition regime* where the importance of slip effects is crucial, and then finally to the conventional *continuum regime*.

Section 3

Description of the geometry, CFD methods, and conditions for use in hypersonic flow

In this section, the methods, setting, and conditions that are used during the hypersonic flow simulation will be explained. This is done to gain trust and confidence in the software and results. This section is devoted to the explanation of each setting of Ansys Fluent, the computational fluid dynamics (CFD) software used in this thesis. Furthermore, the geometry that is used in the simulation will be explained as well.

3.1 Geometry and boundary conditions

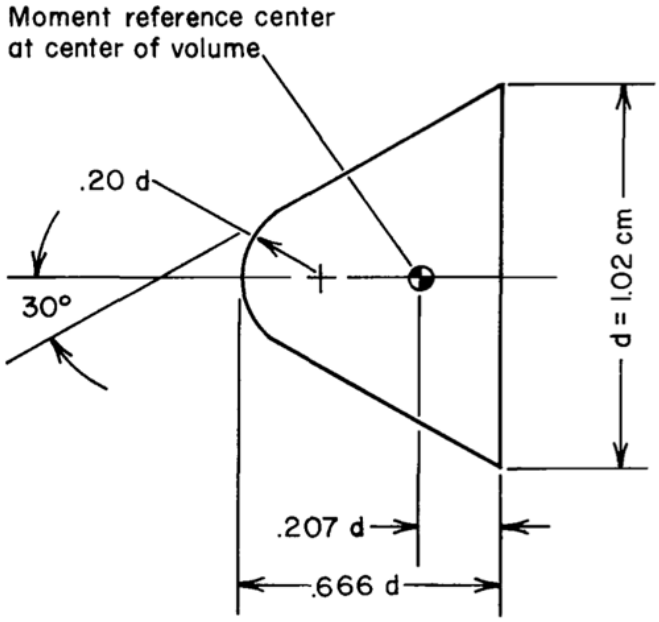

Figure 8. Sketch of the blunted cone *[4]*

Figure 8 is the sketch of the blunted cone from NASA TN which is the same geometry that is simulated in this thesis. In order to reproduce the experiment from NASA, geometry with the same parameters was designed using CAD software and implemented in the 'SpaceClaim'[1] to assign the flow field. Assigned flow field can be seen in Figure 9.

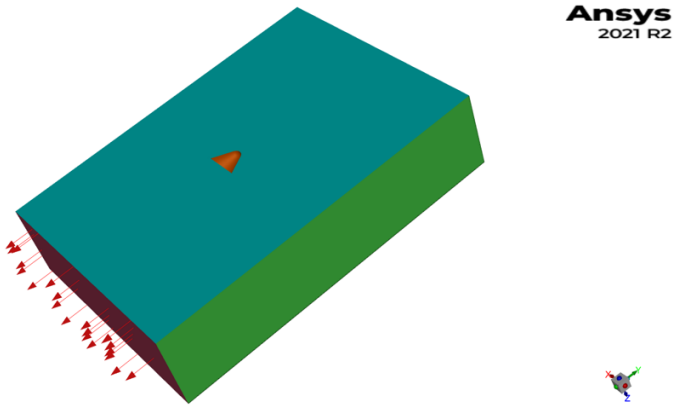

Figure 9. Flow field with boundary conditions

Furthermore, in order to achieve desired results as in NASA TN, following boundary conditions are defined as in Table 1.

Table 1. Boundary conditions

Color	Zone	Boundary condition
Green	Inlet	Pressure far field
Teal	Symmetry	Symmetry
Red	Outlet	Pressure outlet
Orange	Wall	Adiabatic wall

3.2 Methods and conditions

The methods and conditions used in hypersonic CFD simulation are now described to provide background for better understanding the results and to be able to reproduce the same simulations. The methods include solver method, calculation initialization method, solver type, energy, turbulence, radiation, density, specific heat capacity, thermal conductivity, and other boundary conditions. The details can be found in table 2.

[1] SpaceClaim is a solid modelling CAD software that runs on Microsoft Windows and developed by SpaceClaim Corporation. [22]

Table 2. Methods and conditions of CFD

Methods	Settings
Solver method	Finite volume
Solver type	Density-Based
Energy	Energy equation
Calculation Initialization	Hybrid
Turbulence	SST k-omega
Radiation	Discrete Ordinates
Density	Ideal gas
Specific heat	Nasa 9 piecewise polynomial
Thermal conductivity	Kinetic theory
Viscosity	Sutherland
Mach number	11.5, 19.5, 34
Angle of attack	0, 45 [degree]

Ansys Fluent CFD software solves problems using finite volume method. To solve the aerodynamics of the hypersonic flow around the blunted cone would be solved using density-based solver due to the strong coupling between the continuity, momentum, and energy equations. [5] Hybrid initialization is chosen for initialization method to have the initial guess from Ansys Fluent. The aerodynamics of the hypersonic flow was assumed to be calculated using the Reynolds-Averaged Navier-Stokes (RANS) equations. And the flow was assumed to be turbulent, and the two-equation Menter shear-stress transport (SST) model is used. The temperatures were assumed to be in the range where the ideal-gas law is valid for the hypersonic flow. Because of extremely high temperature generated during the flow, discrete ordinates for radiation setting, Nasa 9 piecewise polynomial for specific heat capacity setting, Kinetic theory for thermal conductivity setting, and Sutherland viscosity law for viscosity setting are chosen.

3.2.1 Turbulence setting –SST k-ω Model

Turbulence is the three-dimensional unsteady random motion that is observed in fluids at high Reynolds numbers. While turbulence is principally described by the Navier-Stokes equations, since it requires by far exceed the available computing power it is not feasible to resolve such problems using Direct Numerical Simulation (DNS). Instead, Reynolds-Averaged Navier-Stokes (RANS) is widely used which eliminates all turbulent structures, therefore obtains a smooth variation of the averaged velocity and pressure fields. [6]

The k-ω turbulence model belongs to the RANS family of turbulence models and is one of the most commonly used models to explain the turbulent flow. It is a two-equation model using two transported variables: turbulent kinetic energy (k) which determines the

energy in turbulence and specific turbulent dissipation rate (ω) which determines the rate of dissipation. And one of the variations of k-ω turbulence model is 'SST k-ω turbulence model'. [7]

SST stands for shear stress transport. SST k-ω turbulence model provides a better understanding of flow separation than most RANS models and has a good adversity effect to pressure gradient. [7]

$$\frac{\partial}{\partial t}(\rho k) + \frac{\partial}{\partial x_i}(\rho k u_i) = \frac{\partial}{\partial x_j}\left(\Gamma_k \frac{\partial k}{\partial x_j}\right) + \tilde{G}_k - Y_k + S_k$$

and

$$\frac{\partial}{\partial t}(\rho \omega) + \frac{\partial}{\partial x_i}(\rho \omega u_i) = \frac{\partial}{\partial x_j}\left(\Gamma_k \frac{\partial \omega}{\partial x_j}\right) + G_\omega - Y_\omega + D_\omega + S_\omega$$

where

$\tilde{G}_k$ = the generation of turbulence kinetic energy
G_ω = the generation of ω
Γ_k and Γ_w = the effective diffusivity of k and ω
Y_k and Y_ω = the dissipation of k and ω
S_k and S_ω = user-defined source
D_ω = the cross-diffusion term [8]

3.2.2 Radiation setting – Discrete Ordinates

During the flow in hypersonic speed, the extremely high temperature is inevitably created. And at this point where the temperature is extremely high, the radiation heat transfer becomes significant. Thus, a heat radiation setting plays crucial role during the CFD simulation. In order to bring this phenomenon to CFD, a heat transfer model should be considered. And in order to have an adequate cooling effect, the right radiation transfer model should be chosen.

To choose the suitable model for radiation transfer, the radiation field should be studied, and it is expressed with 'radiative transfer equation', so called RTE. RTE is expressed as following:

$$\frac{dI(\vec{r},\vec{s})}{ds} + (a+\sigma_s)I(\vec{r},\vec{s}) = an^2\frac{\sigma T^4}{\pi} + \frac{\sigma_s}{4\pi}\int_0^{4\pi} I(\vec{r},\vec{s}')\Phi(\vec{s},\vec{s}')\,d\Omega'$$

where

$\vec{r}$ = position vector
$\vec{s}$ = direction vector
$\vec{s}'$ = scattering direction vector
s = path length
a = absorption coefficient
n = refractive index
σ_s = scattering coefficient
σ = Stefan-Boltzmann constant
I = radiation intensity
T = local temperature
Φ = phase function
Ω' = solid angle [9]

RTE is usually impossible to have an exact solution, however, one of the ways to approximate its solution is using Discrete Ordinates radiation method. "Discrete ordinates (DO) radiation model solves the radiative transfer equation (RTE) for a finite number of discrete solid angles, each associated with a vector direction $\vec{s}$ fixed in the global Cartesian system (x, y, z)". [9]

And DO model transforms the radiative transfer equation in the direction $\vec{s}$ as a field equation. Thus,

$$\nabla \cdot (I(\vec{r},\vec{s})\vec{s}) + (a+\sigma_s)I(\vec{r},\vec{s}) = an^2\frac{\sigma T^4}{\pi} + \frac{\sigma_s}{4\pi}\int_0^{4\pi} I(\vec{r},\vec{s}')\Phi(\vec{s},\vec{s}')\,d\Omega'$$

[9]

And since discrete ordinates radiation model uses angular discretization which simplifies the calculation thus requires less powerful computing relatively to the other radiation method, such as Monte Carlo which simulating large ensembles of photon events represented by random samples from probability density functions [10], this radiation model is chosen for this hypersonic simulation.

3.2.3 Density setting – Ideal Gas

Ideal gas law assumes that gas particles have negligible volume and elastic collision interaction properties which neglect intermolecular attraction between the molecules, or atoms. [11] At hypersonic speeds, the gas undergoes significantly high compressible effects, chemical reactions, and thus molecular dissociation which are difficult to verify with the ideal gas model.

However, according to Ansys Fluent, for compressible flows calculations, the ideal gas law is the appropriate density relationship. [12] The equation for the ideal gas law for compressible flows used in Ansys Fluent is sated as following:

$$\rho = \frac{p_{op} + p}{\frac{R}{M_w}T}$$

where,

p = the local relative (or gauge) pressure predicted by Ansys Fluent
p_{op} = the operating pressure [13]

3.2.4 Specific heat capacity setting – NASA 9 Piecewise Polynomial

In hypersonic flow regime, the temperature and pressure conditions are significantly different from those in subsonic and supersonic flow regime. These differences are coming from the extremely high temperature that is created during the flow, thus specific heat is crucial in hypersonic regime. Specific heat can influence on the amount of energy required to increase the temperature of a unit mass of gas which directly connected to the energy transfer. Also, specific heat can directly impact on specific heat capacity, the amount of heat energy needed to raise the temperature of a substance of a unit mass. Especially, specific heat at constant pressure c_p is particularly important in hypersonic flow because it defines the amount of heat needs to be dissipated or controlled during the flow.

The specific heat capacity should be defined when the energy equation is active. And there are different definitions of the heat capacity that are available in Ansys: constant heat capacity, temperature dependent heat capacity, and kinetic theory. [14] In this simulation, NASA 9 Piecewise Polynomial is chosen for specific heat setting since this polynomial function is available for specific heat only and is used in simulating the hypersonic flows. As it is defined in the name, this function is not a constant but a function of temperature. [15]

$$\text{for} \quad T_{min,1} \leq T \leq T_{max,1}: c_p(T) = A_1T^{-2} + A_2T^{-1} + A_3 + A_4T + A_5T^2 + A_6T^3 + A_7T^4$$
$$\text{for} \quad T_{min,2} \leq T \leq T_{max,2}: c_p(T) = B_1T^{-2} + B_2T^{-1} + B_3 + B_4T + B_5T^2 + B_6T^3 + B_7T^4$$

where

A_i and B_i = coefficients [14]

3.2.5 Thermal conductivity setting – Kinetic Theory

In hypersonic calculations, determining the appropriate thermal conductivity setting is crucial depends on the specific context and the level of accuracy required. And in Ansys Fluent, the thermal conductivity must be defined when heat transfer is active especially when energy and viscous flow is being simulated. [16] Since the ideal gas law is activated as density setting, it is recommended to use kinetic theory as the thermal conductivity setting. The equation for kinetic theory used in Ansys Fluent is stated as following:

$$k = \frac{15}{4}\frac{R}{M_w}\mu\left[\frac{4}{15}\frac{c_p M_w}{R} + \frac{1}{3}\right]$$

where

R = the universal gas constant
M_w = the molecular weight
μ = the material's specified or computed viscosity
c_p = the material's specified or computed specific heat capacity [17]

3.2.6 Viscosity Setting – Sutherland Viscosity Law

As it was mentioned earlier in the theoretical section, hypersonic flow is heavily influenced by viscous effect, and is a function of temperature. Therefore, in this hypersonic flow CFD modelling, viscosity model with heat transfer should be selected. And according to Anderson (2006), Sutherland viscosity law is accurate for wide range of temperature and can provide appropriate approach for hypersonic viscous-flow calculation. [4] In this hypersonic CFD model, *Sutherland viscosity law* is chosen.

In 1893 William Sutherland published a relationship between the dynamic viscosity, μ, and the absolute temperature, T, of an ideal gas. This relationship is often referred as 'Sutherland's law' and is resulted from a kinetic theory using an idealized intermolecular-force potential. Since Sutherland's law gives fairly accurate results with a few percent error over a wide range of temperatures, it is still commonly used. The formula can be simplified using two or three coefficients.

Sutherland's law with two coefficients is

$$\mu = \frac{C_1 T^{3/2}}{T + C_2}$$

where

μ = the viscosity in kg/m-s

T = the static temperature in K

C_1 and C_2 = the coefficients / $C_1 = 1.458 \times 10^{-6} \frac{kg}{ms\sqrt{K}}$, $C_2 = 110.4\ K$ [18]

Sutherland's law with three coefficients is

$$\mu = \mu_0 \left(\frac{T}{T_0}\right)^{3/2} \frac{T_0 + S}{T + S}$$

where

μ = the viscosity in kg/m-s

T = the static temperature in K

μ_0 = reference value in kg/m-s / $\mu_0 = 1.716 \times 10^{-5} \frac{kg}{ms}$

T_0 = reference temperature in K / $T_0 = 273.11\ K$

S = an effective temperature in K (Sutherland constant), $S = 110.56\ K$ [18]

Section 4

Performing CFD analysis on the designed body with the evaluation

The results from Ansys Fluent and comparison with the results of the NASA report are presented in this section. Evaluation of the simulation was monitored by observing the convergence of drag forces. Convergence of simulation was determined once the level drag forces level off at steady value.

4.1 Comparison of Meshes

During Computation Fluid Dynamics (CFD) simulations, mesh adaptation is a critical aspect. Mesh adaptation modifies the computational mesh discretizing the selected domain into small elements and improves the accuracy and efficiency of the computation. When the surface and volume mesh are created with the conditions where the user has assigned, the adaptation should be done. In this simulation one of the most important features that has to be captured was the shockwave to compare with the ones from NASA TN. Thus, capturing the boundary layer was one of the important tasks which required a fine-tuned adaptation. And the results are in the below.

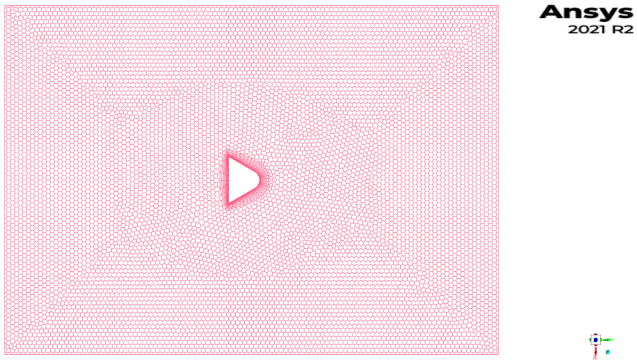

Figure 10. Initial Volume Mesh with 399670 elements

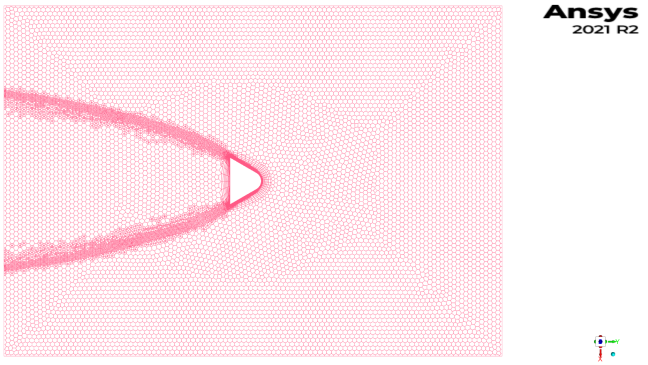

Figure 11. Adopted Volume Mesh with AoA 0 degree with 1497665 elements

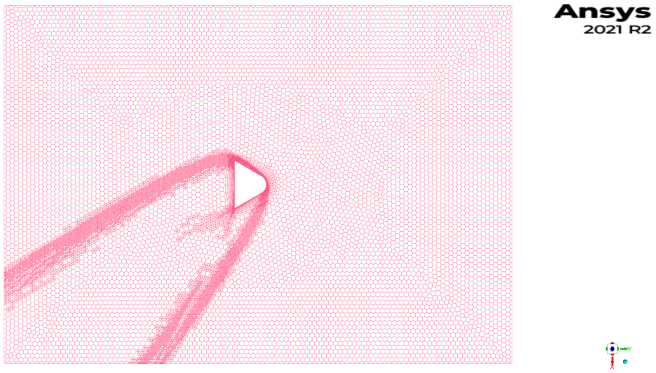

Figure 12. Adopted Volume Mesh with AoA 45 degree with 1941281 elements

As it can be seen in the Figure 10, 11, and 12, meshes are adopted mostly in the region where there is overload of computations. And in order to define those regions more detailed, meshes in those regions are refined as much as possible. From these adopted meshes and with different setting values, the simulations were conducted. And in the following section the results carried out from these meshes will be compared.

4.2 Comparison of the shockwaves

The main purpose of this simulation is to realize the hypersonic flow experiments from NASA TN using CFD simulation tool, Ansys Fluent. And comparing the shockwaves at different Mach number generated throughout the simulation would be the first step to evaluate the success of this simulation. The figures from both NASA TN and Ansys Fluent would be presented at different Mach number: 11.5, 19.5, and 34 respectively, furthermore, two different figures will be overlayed one on another to compared intuitively.

4.2.1 At Mach number 11.5

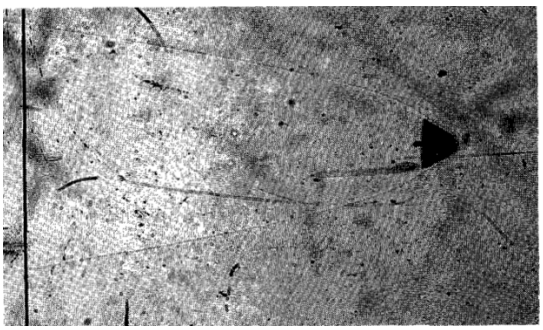

Figure 13. Shockwave at Mach 11.5 from NASA Technical Note *[3]*

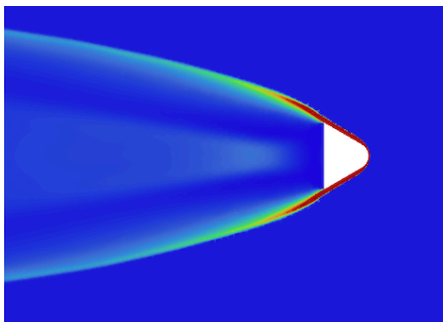

Figure 14. Shockwave at Mach 11.5 from Ansys

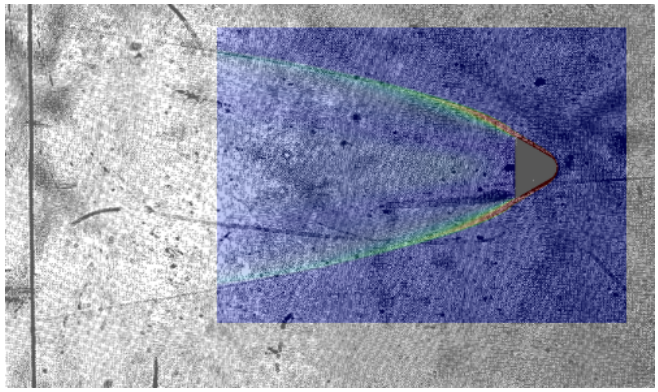

Figure 15. Comparison of Shockwaves at Mach 11.5

As it can be seen in Figure 15, the shockwaves from the NASA TN and Ansys are correlated to each other.

4.2.2 At Mach number 19.5

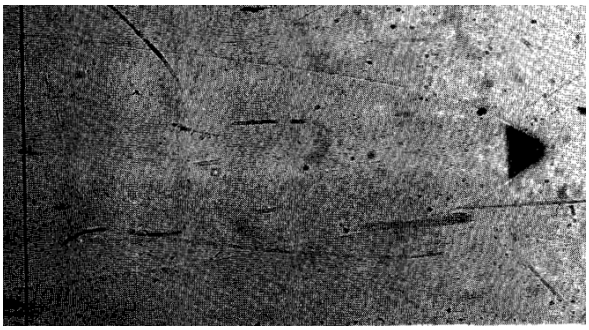

Figure 16. Shockwave at 19.5 from NASA Technical Note *[3]*

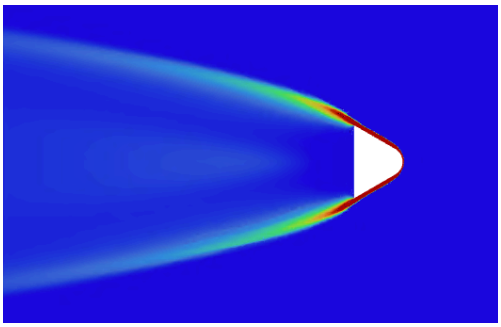

Figure 17. Shockwave at Mach 19.5 from Ansys

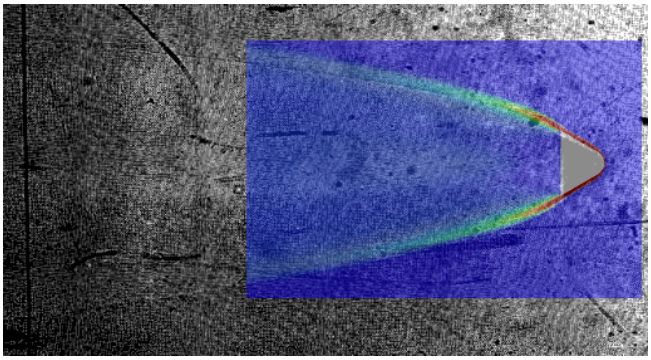

Figure 18. Comparison of Shockwaves at 19.5

As it can be seen in Figure 18, two shockwaves obtained from both NASA TN and Ansys are correlated.

4.2.3 At Mach number 34

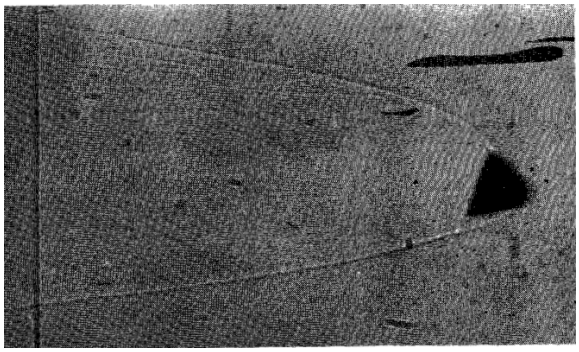

Figure 19. Shockwave at Mach 34 from NASA Technical Note *[3]*

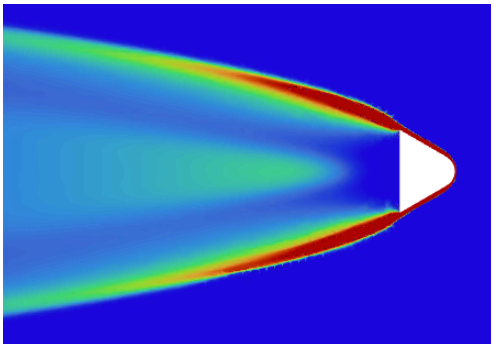

Figure 20. Shockwave at Mach 34 from Ansys

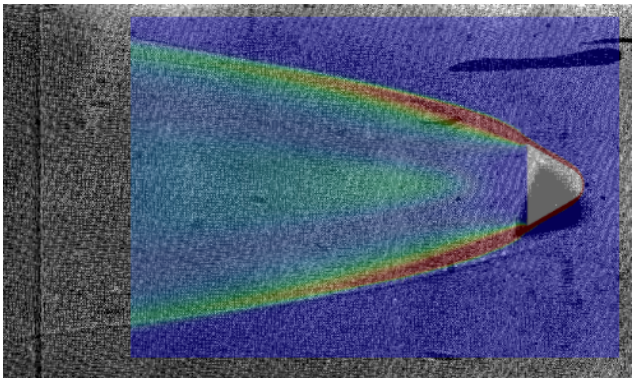

Figure 21. Comparison of Shockwaves at Mach 34

As it can also be seen in Figure 21, the shockwaves from the NASA TN and simulation are correlated as well. Even if the blunted cone body was tilted in the Figure 14 due to its extremely high-speed condition during the experiment, the shockwaves can be observed as identical.

From these direct comparisons of shockwaves at different Mach numbers (11.5, 19.5, and 34), it can be said that the boundary conditions and meshing methods are well assigned for this hypersonic simulation.

4.3 Comparison of velocity, pressure, and temperature fields

In order to find an effect of different angles of attack at the constant Mach number, the simulation was carried out by assigning sines and cosines values for each degree to each component of flow directions at cartesian coordinates (x, y, and z). For example, since the flow of fluid is opposite to y-coordinate, when angle of attack is 0-degree, Y-component of flow direction is '-1' and X-component of flow direction is '0'. For 45-degree, Y-component is '-0,707106781' and X-component is '0,707106781'.

4.3.1 Velocity Field

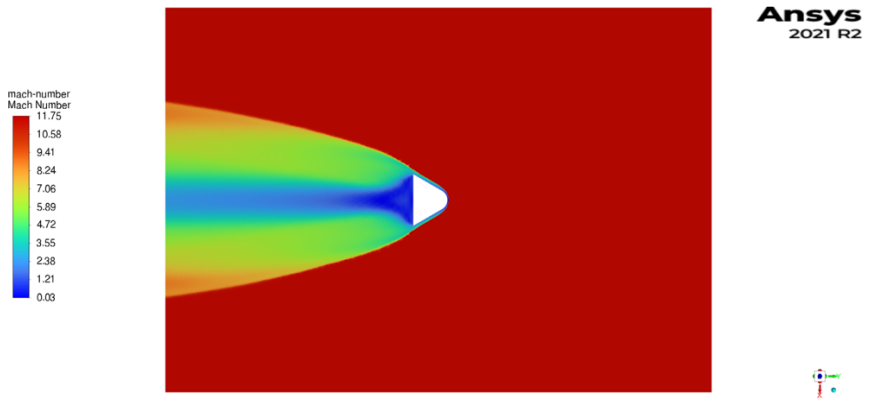

Figure 22. Velocity Field at Mach 11.5 with AoA 0 degree

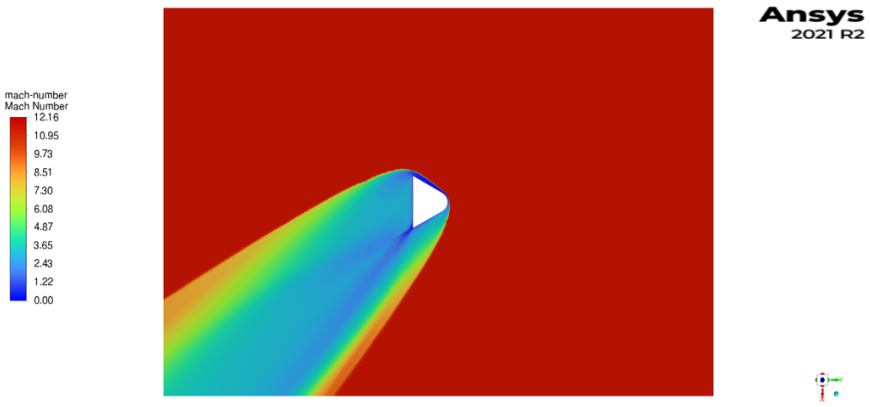

Figure 23. Velocity Field at Mach 11.5 with AoA 45 degree

In Figure 22, velocity value at the tip of the cone is relatively slower than the other region. Because the flow is blocked by the body so that the velocity at the tip slows down. However, as the flow surpasses this region it joins the other flows flowing along the body resulting in increase in the velocity along the body. This phenomenon is happening in Figure 23 as well. Only because the angle of attack is changed to 45 degrees, the principle

is the same. When the flow hits the body it slows down, however then joins the other stream of flow resulting in accelerating thus higher velocity along the body.

4.3.2 Pressure Field

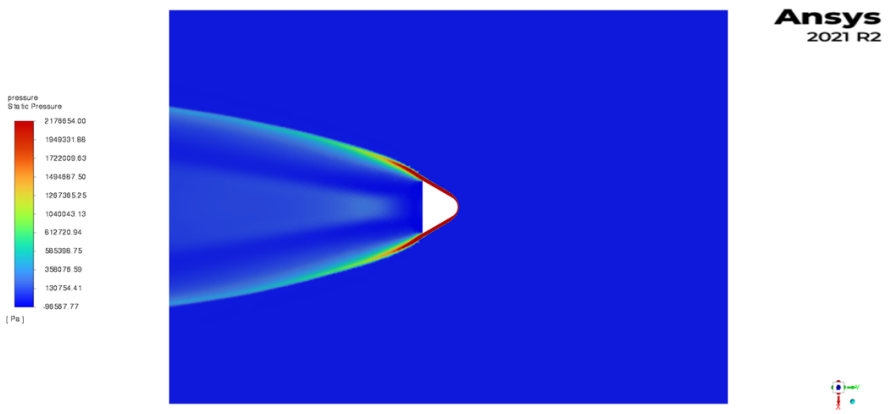

Figure 24. Pressure Field at Mach 11.5 with AoA 0 degree

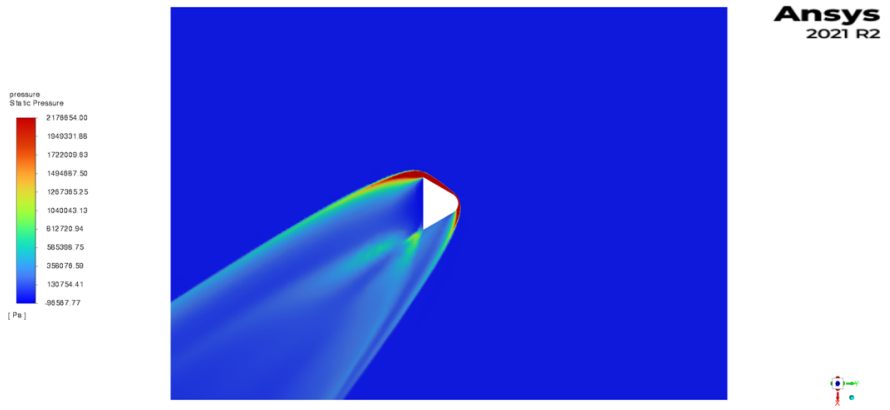

Figure 25. Pressure Field at Mach 11.5 with AoA 45 degree

Secondly, pressure field will be evaluated. In Figure 24, an extremely high pressure is applied to the tip of the cone. As it was mentioned in the velocity field section, flow slows down when the flow hits the body. This will then increase the pressure in that region significantly considering the flow is in hypersonic speed. This extremely high pressure is observed along the surface of the cone and forms very thin pressure layer along the body. Also, the relatively high pressure is created behind the body.

In Figure 25, an extremely high pressure is also applied, however on the side of the cone. Unlike the situation in Figure 24, there is a sudden change in the shape of profile where the flow hits to the body, thus creates quite a huge bump in the pressure field as it can be

seen on the top of the cone. Similarly, a relatively high pressure is also created behind the body.

Surprisingly, as it can be seen in both Figure 24 and Figure 25, the angle of attack is not a main factor of increase in pressure field. Both AoAs have similar static pressure value with 2176654 Pa.

4.3.3 Temperature Field

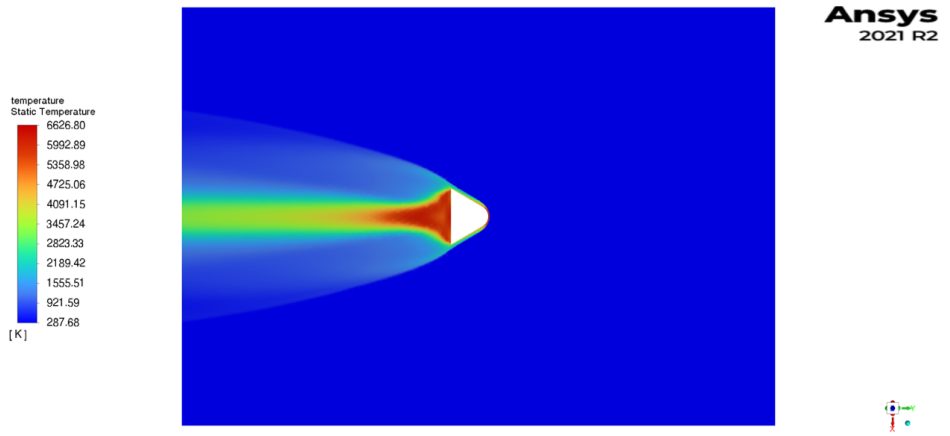

Figure 26. Temperature Field at Mach 11.5 with AoA 0 degree

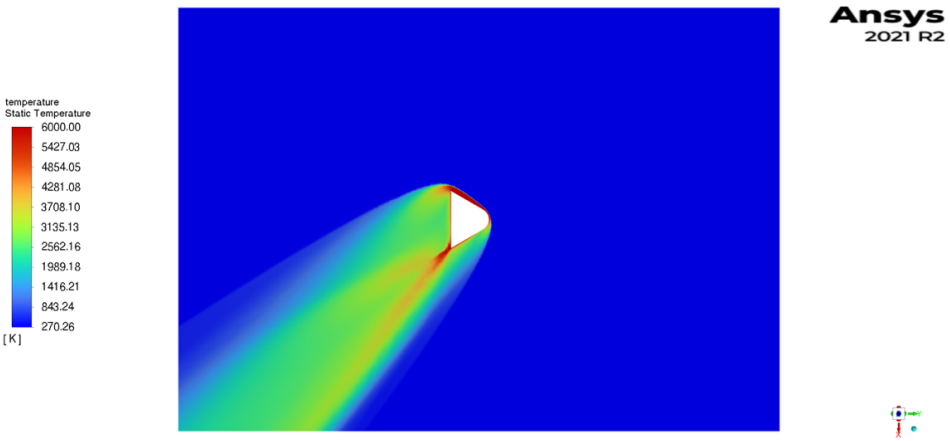

Figure 27. Temperature Field at Mach 11.5 with AoA 45 degree

In Figure 26, the temperature in the region of the tip of the nose reaches around 6600K. And this phenomenon is expected due to the kinetic energy is being dissipated by the influence of friction to the heat. However, there is also the region behind the body where the temperature reaches about 6600K as well.

In Figure 27, the temperature in the region where the flow hits the first reaches the highest. As in Figure 26, there is a region where quite high temperature occurs behind the body with respect to flow direction.

4.4 Comparison of velocity, pressure, and temperature fields at different Mach number: 11.5, 19.5, and 34.

4.4.1 Velocity Field

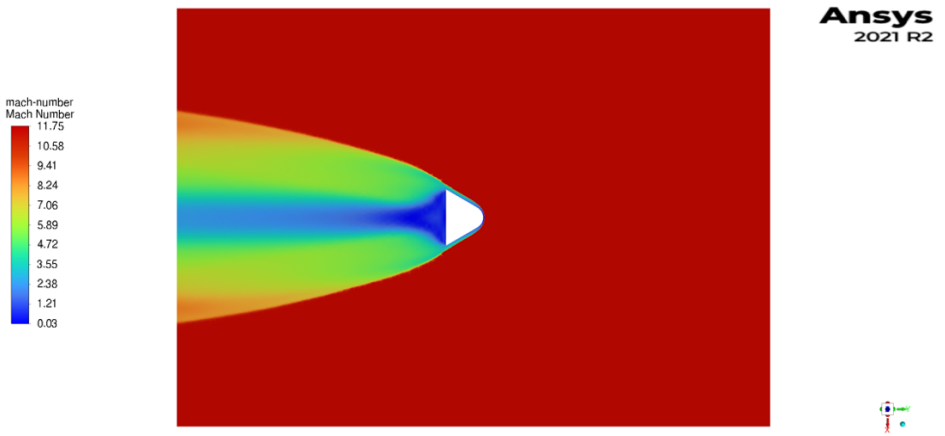

Figure 28. Velocity Field at Mach 11.5

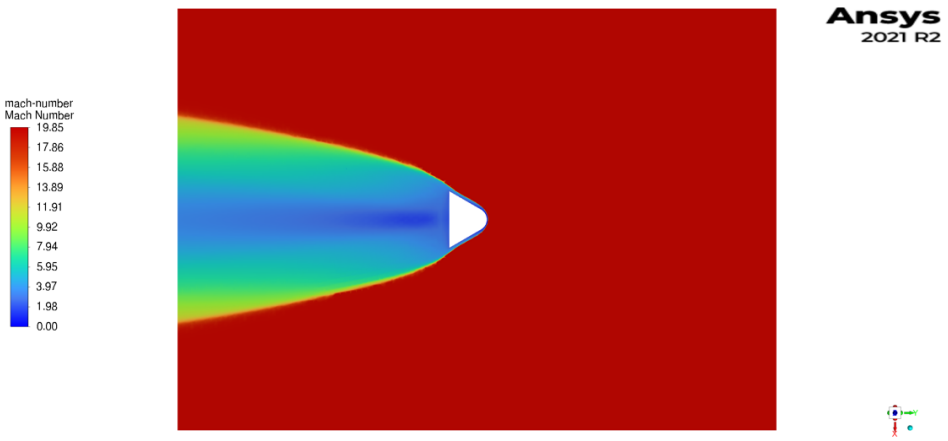

Figure 29. Velocity Field at Mach 19.5

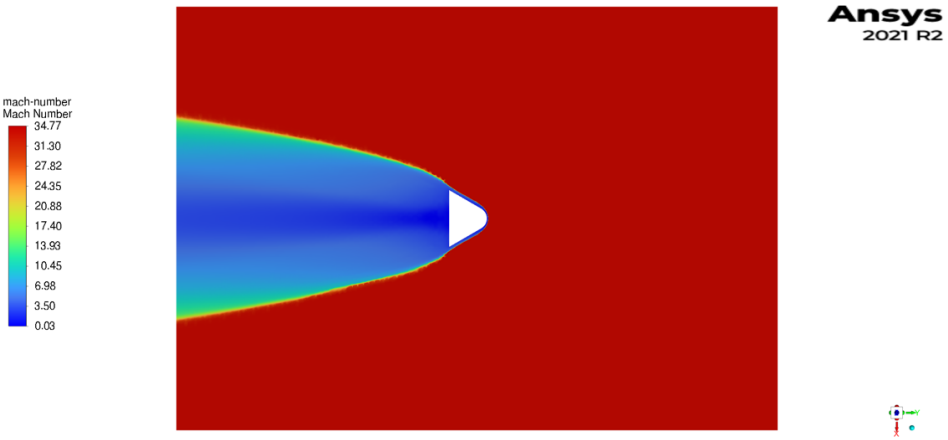

Figure 30. Velocity Field at Mach 34

From figure 28, 29, and 30, it can be seen that the shockwaves become thinner and larger gradient appears as Mach number increases from 11.5 to 34.

4.4.2 Pressure Field

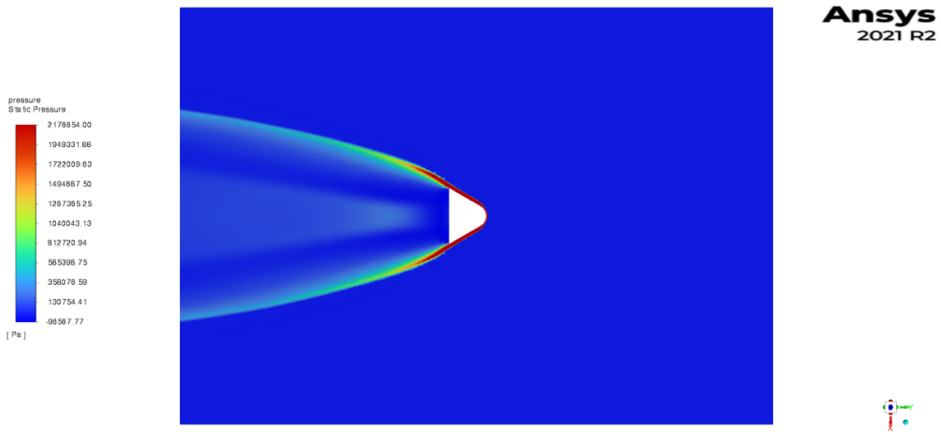

Figure 31. Pressure Field at Mach 11.5

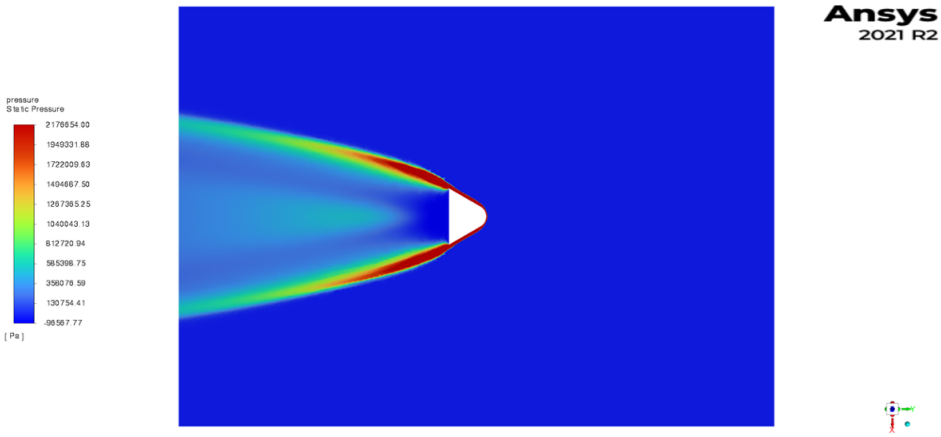

Figure 32. Pressure Field at Mach 19.5

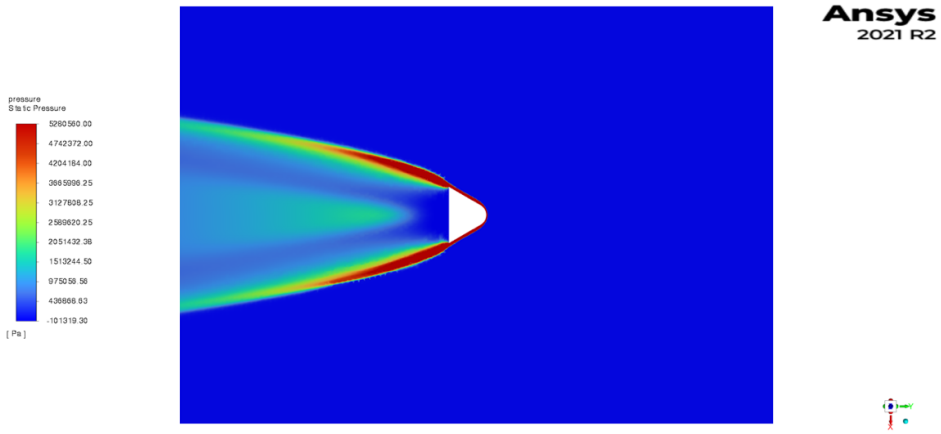

Figure 33. Pressure Field at Mach 34

4.4.3 Temperature Field

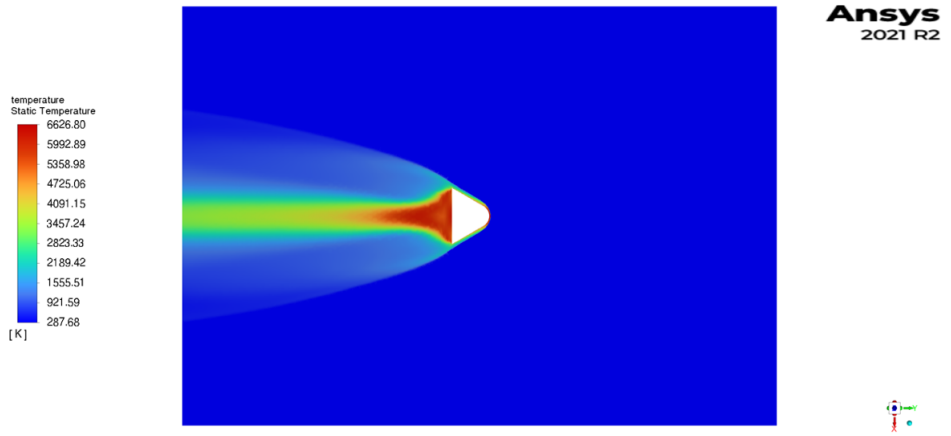

Figure 34. Temperature Field at Mach 11.5

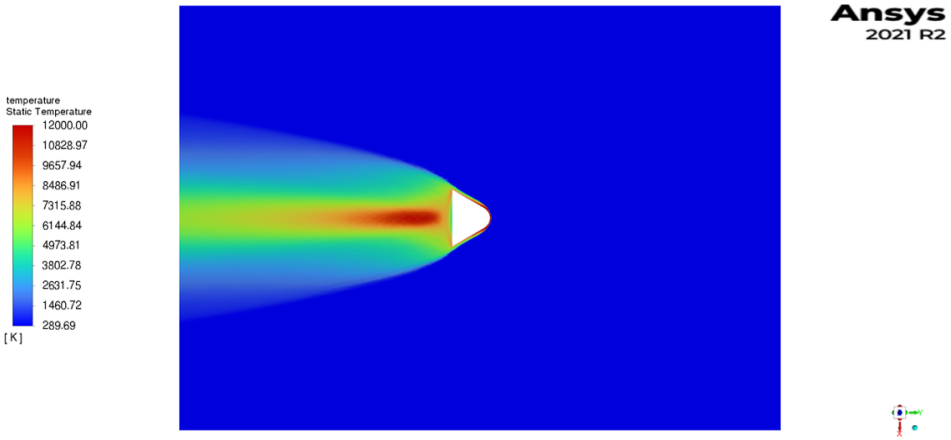

Figure 35. Temperature Field at Mach 19.5

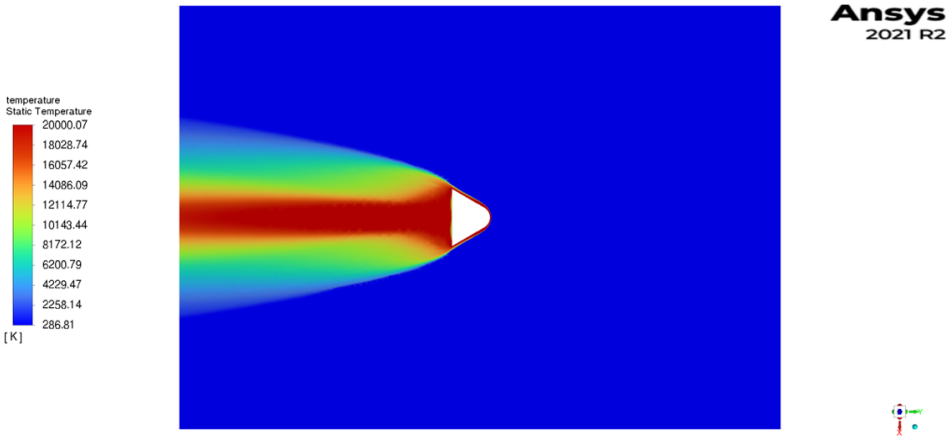

Figure 36. Temperature Field at Mach 34

4.5 Comparison of Pitching moment, Drag, and Lift Coefficients

Using the data from NASA TN, the results of the hypersonic simulation have been evaluated. Pitching moment coefficient and drag coefficient are directly compared with NASA data, and lift coefficient has been evaluated and is presented by itself.

4.5.1 Pitching Moment Coefficient

Table 3 shows the results of pitch moment coefficient from both NASA TN and Ansys Fluent CFD simulation. The coefficients from simulation are generally higher than the results from NASA TN.

Table 3. Pitch moment coefficient from NASA and Ansys Fluent *[3]*

Angle of Attack [°]	0	5	10	15	20	25	30
NASA	0	0,0201	0,0406	0,0571	0,0705	0,0783	0,0810
Ansys Fluent	0	0,0241	0,0437	0,0576	0,0685	0,0778	0,0855
Error [%]	0	16,59	7,64	0,88	2,84	0,64	5,56

Figure 37 shows the pitching moment coefficient at different AoA from both NASA TN and Ansys Fluent simulation. Even if the results have error as it can be seen table 3, both graphs are comparable.

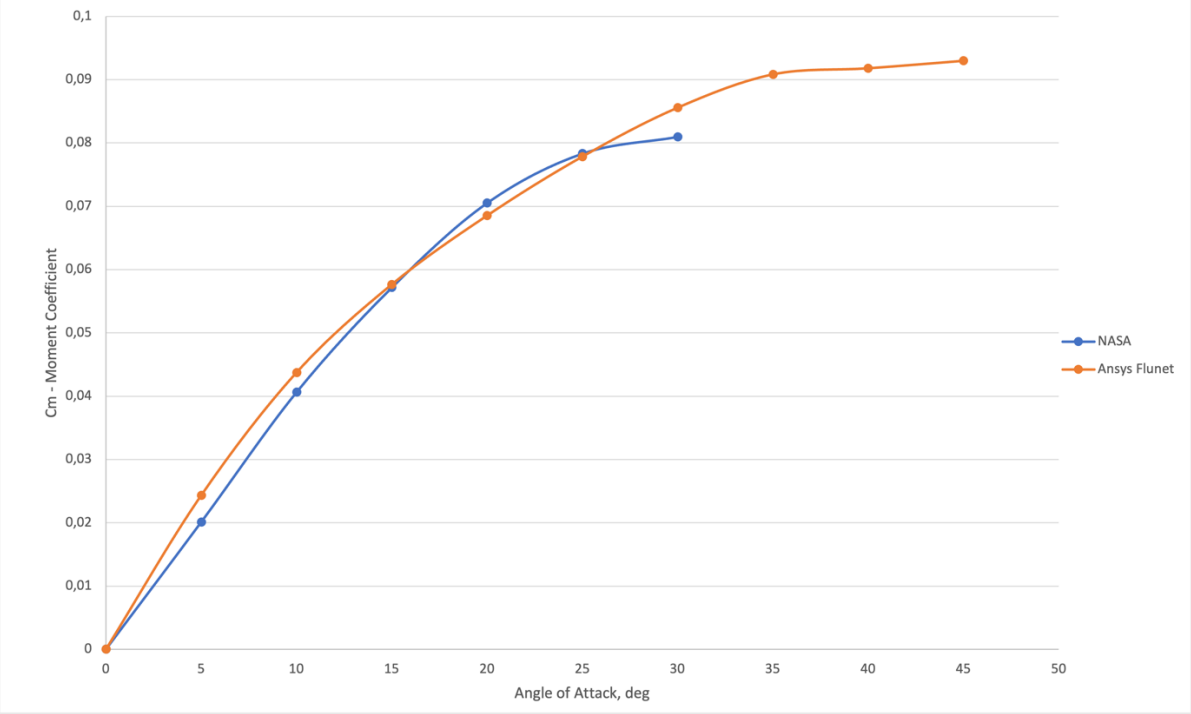

Figure 37. Pitching moment coefficient from NASA and Ansys Fluent *[3]*

4.5.2 Drag Coefficient

Direct comparison would be difficult for the drag coefficient. In NASA paper, root-mean-square resultant angle of attack is used due to the fluctuation of the blunted cone at hypersonic flow experiment. However, essentially there isn't much difference between RMS resultant AoA and normal AoA, RMS resultant AoA is used for the data analysis.

Table 4 shows the results of drag coefficient from both NASA TN and Ansys Fluent CFD simulation. As it was said earlier, both results are processed with different AoA, thus in order to have a clear look both results are presented in one figure.

Table 4. Drag coefficient from NASA and Ansys Fluent *[3]*

NASA		**Ansys Fluent**	
RMS Resultant AoA [°]	Drag coefficient	AoA [°]	Drag coefficient
5,750280566	0,582404118	0	0,547243865
8,291830116	0,574764479	5	0,55745938
9,401163449	0,604097812	10	0,586685149
9,957971686	0,59179408	15	0,628805859
12,81284942	0,638177606	20	0,677230997
15,03349292	0,67194852	25	0,729620386
22,25552638	0,719464607	30	0,78234964
		35	0,829075046
		40	0,859145709
		45	0,874692908

Figure 38 shows the drag coefficient at different AoA from both NASA TN and Ansys Fluent simulation. To check how accurate the simulation was, the drag coefficient at AoA 10, 15, and 20 are read, and used in calculating errors. Table 5 shows the readings for AoA 10, 15, and 20 from NASA TN and Ansys Fluent, and their errors.

Table 5. Error calculation of Drag coefficient *[3]*

Angle of Attack [°]	**10**	**15**	**20**
NASA	0,608	0,657	0,708
Ansys Fluent	0,587	0,629	0,677
Error [%]	3,51	4,29	4,35

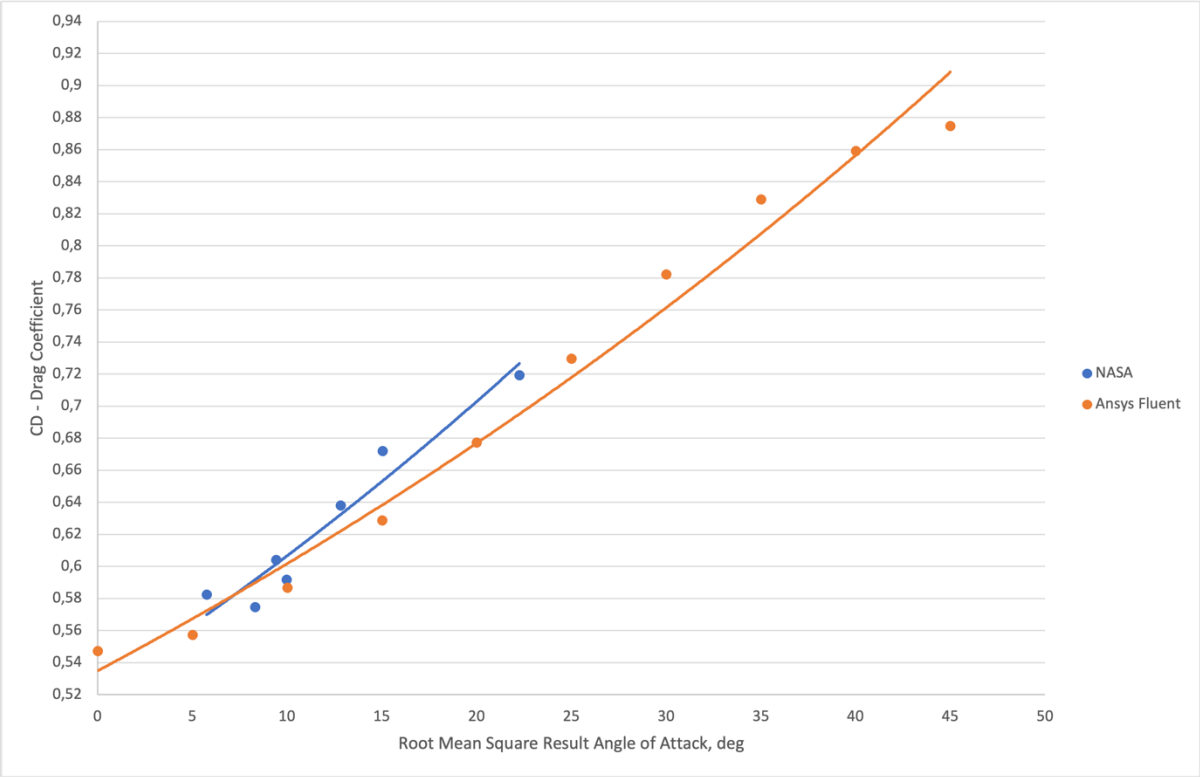

Figure 38. Drag coefficient from NASA and Ansys Fluent *[3]*

4.5.3 Lift Coefficient

Table 5 shows the results of lift coefficient from Ansys Fluent CFD simulation. The lift coefficient was not evaluated in the NASA TN.

Table 6. Lift coefficient from NASA and Ansys Fluent *[3]*

AoA [°]	0	5	10	15	20	25	30	35	40	45
C_L	0	29,98	52,13	64,54	68,87	68,25	61,74	49,33	31,16	10,19

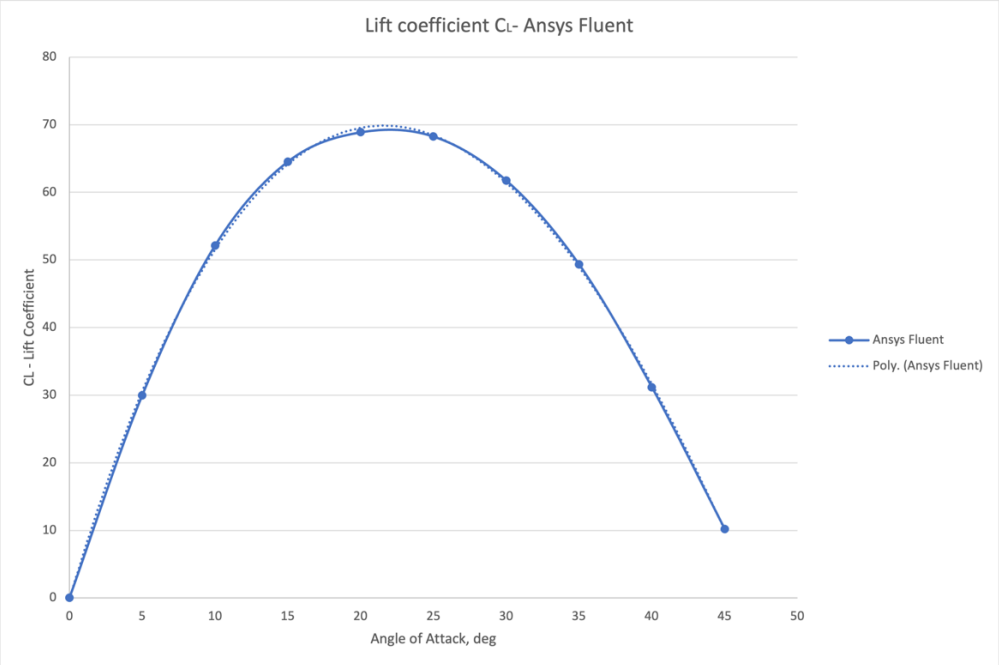

Figure 39. Lift coefficient from Ansys Fluent

Section 5

Conclusions and discussions

The answer to the main thesis question and subquestions are presented in this chapter. To improve the results presented in chapter 4, this chapter will also provide some discussion for future research.

5.1 Conclusions

In the introduction of this thesis, the thesis questions and goals were introduced. In conclusion section, these questions and goals will be answered. The question goal was:

Compared to the data between NASA technical note, how accurate the CFD simulation is?

To answer this question, first of all, subgoals were determined. First, definition of hypersonic flow was determined. Hypersonic flow has characteristics of thin shock layers, entropy layer, viscous interaction, high-temperature flow, and low-density flow. Then, appropriate boundary conditions and settings for hypersonic flow simulations was chosen and validated as follows:

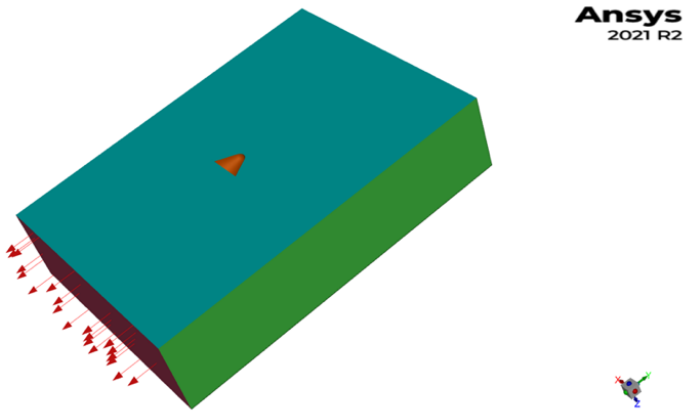

Figure 40. Flow field with boundary conditions

Table 7. Boundary conditions

Color	Zone	Boundary condition
Green	Inlet	Pressure far field
Teal	Symmetry	Symmetry
Red	Outlet	Pressure outlet
Orange	Wall	Adiabatic wall

Table 8. Methods and conditions of CFD

Methods	Settings
Solver method	Finite volume
Solver type	Density-Based
Energy	Energy equation
Calculation Initialization	Hybrid
Turbulence	SST k-omega
Radiation	Discrete Ordinates
Density	Ideal gas
Specific heat	Nasa 9 piecewise polynomial
Thermal conductivity	Kinetic theory
Viscosity	Sutherland
Mach number	11.5, 19.5, 34
Angle of attack	0, 45 [degree]

As the settings for simulation is done, simulation has been conducted. Then, as in Section 4, the results can be obtained.

The main thesis question is answered by answering the subquestions. The answer to the main question is mainly a comparison of results from both the CFD simulation and the NASA TN.

The first subquestion was: *How similar the shockwaves from both NASA TN and simulation?* Section 4.2 has shown the similarity of the shockwaves from both NASA TN and CFD simulation. In the overlayed figures, shockwaves at different Mach numbers were correlated. Thus, the boundary conditions and settings for the blunted geometry at different Mach numbers are well selected.

The second subquestion was: *How accurate the pitch-moment coefficients are compared to that of NASA TN?* Section 4.5.1 has shown the results of pitch-moment coefficients from both sources. Even if the curves presented in Figure 37 are not exactly identical, the trend lines share the similar tendency. The errors are calculated in Table 3. Although the biggest error is 16,59% at lower angle, however, error at higher angles remains at quite reasonable values such as 0,64%.

The third subquestion was: *How accurate the drag coefficients are compared to that of NASA TN?* Section 4.5.2 has shown the results of drag coefficients from both sources. As for the pitch-moment coefficients, the curves for drag coefficients in Figure 38 are not identical. However, they also share the similar trend tendency. The errors are calculated in Table 5. Although only 3 angles of attack were able to be compared with the CFD simulation results due to lack of data from NASA TN, it provided general idea of the errors. The error for those angles remains around at 4% which is reasonable.

5.2 Discussions

The obtained results in this thesis can be further improved. Possible improvements of the quality of the work are given in this section.

Meshing resolution

When it comes to the discrepancy with the experiment and the CFD simulation, the first possible of error is with the meshing. In order to capture the correct physical phenomenon during the high load computation such as hypersonic flow, the appropriate setting of meshing is crucial. This can be done with mesh sensitivity analysis. This refers to conduct the same simulation with different sets of resolution or quality and see how much they converge according to the meshes. Even if this was done during this simulation, if more organized mesh sensitivity analysis is done the results can be further improved.

Conditions and settings

Conditions and settings also can be source of discrepancy. Even if conditions and settings used in the simulation are recommended by Ansys Fluent, appropriate validation is required to conclude the results. Even if the results of the CFD simulation is fairly close to that of NASA TN, there are few points that need to be mentioned.

First, the chemical reaction in the flow field was not considered. In section 2.4, the chemical reaction plays a crucial role when it comes to hypersonic flow regime due to its extreme temperature. In order to capture this phenomenon, turning on Two-Temperature model will definitely help the accuracy of the result of the CFD simulation.

The other one is boundary condition of the wall. Since there is no information of the body in NASA TN, it was not certain what the temperature was of the body during the experiment. Thus, in this CFD simulation, adiabatic wall temperature with '0' heat flux is used, and this might have created some discrepancy during the simulation. By assigning different heat flux or assigning the specific temperature on the wall could influence the results of the simulation, and then can further improve the accuracy of the simulation as well.

Bibliography

[1] NewScientist, "9 quotes that tell the dramatic story of supersonic flight," 22 February 2017. [Online]. Available: https://www.newscientist.com/article/2121765-9-quotes-that-tell-the-dramatic-story-of-supersonic-flight/.

[2] WIKIPEDIA, "Rockwell X-30," [Online]. Available: https://en.wikipedia.org/wiki/Rockwell_X-30.

[3] P. F. Intrieri, "Experimental Stability and Drag of A Pointed and A Blunted 30 Half-angle Cone at Mach Numbers from 11.5 to 34 in Air," National Aeronautics and Space Administration, Washington D.C., 1966.

[4] J. D. A. Jr., Hypersonic and High Temperature Gas Dynamics, American Institute of Aeronautics and Astronautics, 2006.

[5] Ansys, "16.1. Introduction to Hypersonic Flows," 2023. [Online]. Available: https://ansyshelp.ansys.com/account/secured?returnurl=/Views/Secured/corp/v232/en/flu_ug/flu_ug_hsn_intro.html.

[6] Ansys, "13.1. Introduction," 2023. [Online]. Available: https://ansyshelp.ansys.com/account/secured?returnurl=/Views/Secured/corp/v212/en/flu_ug/flu_ug_sec_turb_intro.html.

[7] "K-Omega and K-Omega SST," SIMSCALE, 2021. [Online]. Available: https://www.simscale.com/docs/simulation-setup/global-settings/k-omega-sst/.

[8] Ansys, "4.5.2 Shear-Stress Transport (SST) k-omega Model," 2009. [Online]. Available: https://www.afs.enea.it/project/neptunius/docs/fluent/html/th/node67.htm.

[9] Ansys, "5.3.6. Discrete Ordinates (DO) Radiation Model Theory," Ansys, 2021. [Online]. Available: https://ansyshelp.ansys.com/account/secured?returnurl=/Views/Secured/corp/v212/en/flu_th/flu_th_sec_mod_disco.html.

[10] H. a. H. J. R. Ertürk, "Monte Carlo Methods for Radiative Transfer," in *in Handbook of Thermal Science and Engineering*, Springer International Publishing, Cham., 2017, p. 1–43.

[11] WIKIPEDIA, "Ideal gas law," [Online]. Available: https://en.wikipedia.org/wiki/Ideal_gas_law.

[12] Ansys, "8.3.1. Defining Density for Various Flow Regimes," 2023. [Online]. Available: https://ansyshelp.ansys.com/account/secured?returnurl=/Views/Secured/corp/v212/en/flu_ug/flu_ug_density_set.html?q=ideal%20gas.

[13] Ansys, "8.3.7. Ideal Gas Law for Compressible Flows," 2021. [Online]. Available: https://ansyshelp.ansys.com/account/secured?returnurl=/Views/Secured/corp/v212/en/flu_ug/flu_ug_sec_density_ideal.html.

[14] Ansys, "8.7. Specific Heat Capacity," 2023. [Online]. Available: https://ansyshelp.ansys.com/account/secured?returnurl=/Views/Secured/corp/v232/en/flu_ug/flu_ug_sec_cp.html?q=nasa.

[15] Ansys, "8.2.4. Inputs for NASA-9-Piecewise-Polynomial Functions," 2021. [Online]. Available: https://ansyshelp.ansys.com/account/secured?returnurl=/Views/Secured/corp/v212/en/flu_ug/flu_ug_sec_material_nasa-9_piece.html.

[16] Ansys, "8.5. Thermal Conductivity," 2021. [Online]. Available: https://ansyshelp.ansys.com/account/secured?returnurl=/Views/Secured/corp/v212/en/flu_ug/flu_ug_sec_thermcond.html?q=3.2.5Thermal%20conductivity.

[17] Ansys, "8.5.3. Thermal Conductivity Using Kinetic Theory," 2021. [Online]. Available: https://ansyshelp.ansys.com/account/secured?returnurl=/Views/Secured/corp/v212/en/flu_ug/x1-7550009.11.3.html.

[18] Ansys, "8.4.2. Viscosity as a Function of Temperature," 2021. [Online]. Available: https://ansyshelp.ansys.com/account/secured?returnurl=/Views/Secured/corp/v212/en/flu_ug/x1-7350009.4.2.html?q=sutherland.

[19] T. A.Edwards, "Fluid/Chemistry modeling for Hypersonic Flight Analysis," Pergamon Press Ltd, Moffett Field, California, U.S.A, 1992.

[20] J. v. Oostrom, "Effects of increasing aerothermmodynamic fidelity on hypersonic trajectory optimisation for flight testing purposes," TUDelft, 2015.

[21] curiosityFluids, "Sutherland's Law," [Online]. Available: https://curiosityfluids.com/2019/02/15/sutherlands-law/#:~:text=According%20to%20Anderson%20(2006)%2C,hypersonic%20viscous%2Dflow%20calculations"..

[22] WIKIPEDIA, "SpaceClaim," [Online]. Available: https://en.wikipedia.org/wiki/SpaceClaim.